INTRODUCTION TO THE ESTIMATION OF THE LIFT COEFFICIENTS AT ZERO ANGLE OF ATTACK AND AT MAXIMUM LIFT FOR AEROFOILS WITH HIGH-LIFT DEVICES AT LOW SPEEDS

1. NOTATION AND UNITS

The notation given here is restricted to that required for this Item, with the exception of Section 7. For some of the notation in that Section and for the complete notation required in the use of the individual Items referred to herein, reference should be made to the appropriate Items (*i.e.* References 6 and 8 to 12).

		SI	*British*
C_L	lift coefficient, based on c		
C_{Lm}	maximum lift coefficient of aerofoil with high-lift devices deployed, based on c		
C_{LmB}	maximum lift coefficient of basic aerofoil, based on c		
C_{L0}	lift coefficient at zero angle of attack for aerofoil with high-lift devices deployed, based on c		
C_{L0B}	lift coefficient at zero angle of attack for basic aerofoil, based on c		
ΔC_{Lm}	increment in maximum lift coefficient due to deployment of high-lift devices, based on c		
ΔC_{Lml}	increment in maximum lift coefficient due to deployment of leading-edge high-lift device, based on c		
ΔC_{Lmt}	increment in maximum lift coefficient due to deployment of trailing-edge flap, based on c		
ΔC_{L0}	increment in lift coefficient at zero angle of attack due to deployment of high-lift devices, based on c		
ΔC_{L0l}	increment in lift coefficient at zero angle of attack due to deployment of leading-edge high-lift device, based on c		
ΔC_{L0t}	increment in lift coefficient at zero angle of attack due to deployment of trailing-edge flap, based on c		
c	basic aerofoil chord (*i.e.* chord with high-lift devices undeployed)	m	ft
c'	extended aerofoil chord (*i.e.* chord with high-lift devices deployed)	m	ft
t	maximum thickness of aerofoil	m	ft

Issued December 1994
With Amendment A, July 1995

| α | angle of attack of basic aerofoil chord line relative to free stream | rad | rad |

Subscripts

$( )_{expt}$ denotes experimental value

$( )_{pred}$ denotes predicted value

2. INTRODUCTION

This Item provides an introduction to aerofoil lift and the effects of high-lift device deployment at low speeds. It centres in particular on the effects on the lift coefficient at zero angle of attack, C_{L0}, and on the maximum lift coefficient, C_{Lm}. The Item acts as an introduction to, and a link between, the Item (Reference 6) for the basic aerofoil[*] and the Items (References 8 to 12) in the complete series dealing with the incremental effects, ΔC_{L0} and ΔC_{Lm}, of high-lift device deployment. The Item also describes how the incremental effects on C_{L0B} and C_{LmB} for the basic (*i.e.* plain) aerofoil are used to give the total values C_{L0} and C_{Lm}.

Section 3 describes the lift development on basic aerofoils up to the stall and briefly discusses the various stall categories. It goes on to consider the effects of high-lift device deployment on aerofoil lift characteristics, with particular reference to the zero angle of attack and maximum lift cases.

Section 4 describes the procedure whereby the contributions obtained from References 6 and 8 to 12 are used to estimate the total values C_{L0} and C_{Lm}. A guide to the location of the information for the basic aerofoil and each of the high-lift devices is presented in tabular form.

Section 5 provides a discussion of the applicability and an assessment of the overall accuracy of the methods given for C_{L0} and C_{Lm}. Section 6 gives the References and Section 7 gives two examples. The first example provides a typical illustration of the calculation procedure. Due to a lack of experimental data none of the Data Items specifically treats the practical case of a tabbed-Fowler flap. Consequently, a second example has been included to show how the methods of Reference 11 for a single-slotted flap and Reference 9 for a plain flap may be combined, using the principles established for double-element flaps in Reference 12, to treat the case of a tabbed-Fowler flap.

3. LIFT DEVELOPMENT UP TO THE STALL

At low speeds the two-dimensional flow over an aerofoil, with high-lift devices undeployed, normally remains attached at small angles of attack and the increase of lift coefficient with angle of attack is effectively linear. At a certain angle of attack, dependent on the section geometry and the free-stream conditions, flow separation starts. Further increase in angle of attack causes progressive growth of the separated region and reduction in the slope of the lift curve until a maximum lift coefficient, C_{LmB}, is reached, and the aerofoil stalls. At still higher angles of attack, the lift is reduced, perhaps catastrophically. The main types of stall are discussed briefly in Section 3.1.

---

[*] The term "basic aerofoil" refers to an aerofoil with high-lift devices undeployed; it is synonymous with the term "plain aerofoil" that is sometimes used.
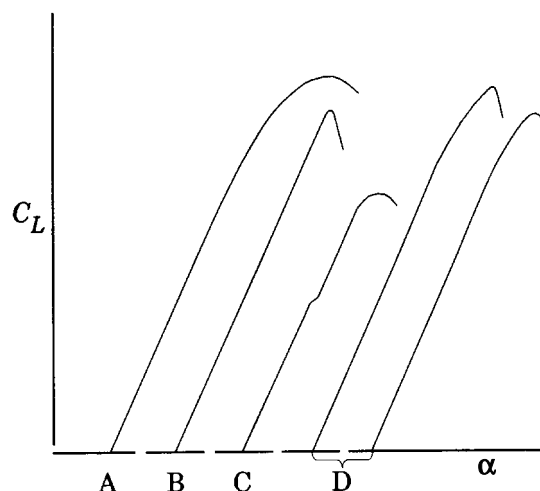
The deployment of high-lift devices affects the lift curve of an aerofoil through changes in the lift coefficient at zero angle of attack, in the point and nature of departure from the near-linear characteristic at low angles of attack and in the maximum lift coefficient. Leading-edge and trailing-edge devices affect lift on an aerofoil in two-dimensional flow in different ways.

The major effect of a leading-edge device is to delay the onset of leading-edge separation, thus increasing the lift attainable before the stall. The major effect of a trailing-edge device on the other hand is to increase the camber of the aerofoil with a consequent increase in lift at a given angle of attack. The use of properly designed slots between the elements of a trailing-edge device further enhances the maximum lift attainable. Typical lift curves associated with various high-lift devices are considered in Section 3.2.

Although the free-stream flow past an aerofoil with high-lift devices deployed may be low-speed, the local flow around a leading-edge slat, for example, can attain supersonic velocities. Compressibility effects can therefore be important.

3.1   Stall of Basic Aerofoil

There are various types of stall related to where flow separations occur on the aerofoil. Four distinct types of stall are identified, having typical lift versus angle of attack curves of the type shown in Sketch 3.1, see Item No. 66034 (Reference 1).

Sketch 3.1   Aerofoil stall classification

Type A: Trailing-edge stall

Trailing-edge stall is due to separation moving forward from the trailing edge as angle of attack increases. This is typical of thick aerofoils (thickness-chord ratio $t/c = 0.15$, say) having a well-rounded suction peak and moderate adverse pressure gradient. A rounded maximum to the lift curve is probable.

Type B: Leading-edge stall

On moderately thin sections, the laminar boundary layer may separate at a particular angle of attack with re-attachment of the shear layer enclosing a "short" bubble followed by a turbulent boundary layer. At a critical angle of attack, less than that at which the flow would break down at the trailing edge, the bubble bursts, giving a sudden fall in lift coefficient. This is typical of sections having t/c between about 0.06 and 0.09.

Type C: Thin aerofoil stall

On very thin sections after initial laminar separation with re-attachment occurring further downstream, a "long" bubble is formed which extends with increasing angle of attack. The lift curve has a discontinuous slope when the bubble first forms, which is followed by a rounded maximum when the bubble has reached the trailing-edge, with subsequent detachment and loss of lift. This is typical of sections having t/c below 0.05, say.

Type D: Combined stall

Here, both laminar separation at the leading edge and turbulent separation at the trailing edge occur before C_{LmB} is reached. The lift curves vary in character and two possibilities, characterised by a sharp or rounded maximum, are depicted in Sketch 3.1. This type of stall is the least common and a typical value of t/c is 0.12.

Fuller details of the nature of these types of stall and the effects on aerofoil characteristics are given in References 1 to 3.

3.1.1   Data Item

It has proved possible to define empirical relationships for estimating the maximum lift coefficient, C_{LmB}, in terms of specified geometric characteristics of the aerofoil, Reynolds number and Mach number for smooth or rough surfaces, see Item No. 84026 (Reference 6). A method for estimating the lift coefficient at zero angle of attack, C_{L0B}, is also included.

3.2   Effects of Deploying High-Lift Devices

The rise of C_L between C_{L0} and C_{Lm} is dependent on the stall characteristics. The effects of deploying plain leading-edge and trailing-edge flaps may, in the first instance, be interpreted partly as those of modified camber. These will produce small decrements in the lift coefficient at zero angle of attack for leading-edge flaps, but major increments for trailing-edge flaps. The increment in lift coefficient between zero angle of attack and maximum lift can also change significantly from that for the basic aerofoil. For example, many high-lift systems comprise two or more elements with chord extensions and slots between the elements in the deflected settings. Although the resultant changes in lift coefficient at zero angle of attack for such systems are significant, the effects on the lift coefficient increment between zero angle of attack and maximum lift due to the complex flow around the multiple elements can predominate. Furthermore, boundary layer separation may occur on any element, thus adding to the complexity. The number of independent parameters is so large in such cases that the complete correlation of test data is not practical. Fortunately, it is possible to simplify the problem by making independent estimates of the effects of each element in turn and summing the results, as described in Reference 4.

Sketch 3.2 shows the lift curves of a particular aerofoil without and with typical high-lift devices, such as those illustrated in Sketch 3.3. The lift coefficient, C_L, is referred to the chord of the basic aerofoil and the increased slopes for the multi-element devices are primarily due to chord extensions. The angle of attack, α, is defined as that of the undeflected part of the aerofoil. Brief outlines of the dominant physical processes affecting the lift curves are given below, but for a more extensive discussion see References 5 and 7.

Leading-edge devices (Sketch 3.3a) reduce the lift coefficient at zero angle of attack due to the negative camber near the nose; the consequent reduction in peak suction allows a significant increase in the angle of attack at which leading-edge separation occurs, thus increasing the maximum lift coefficient. Such devices have a comparatively small effect on trailing-edge flow conditions.

The slot of a slotted leading-edge flap (slat or vented Krüger flap, Sketch 3.3a(iii)) provides a means of
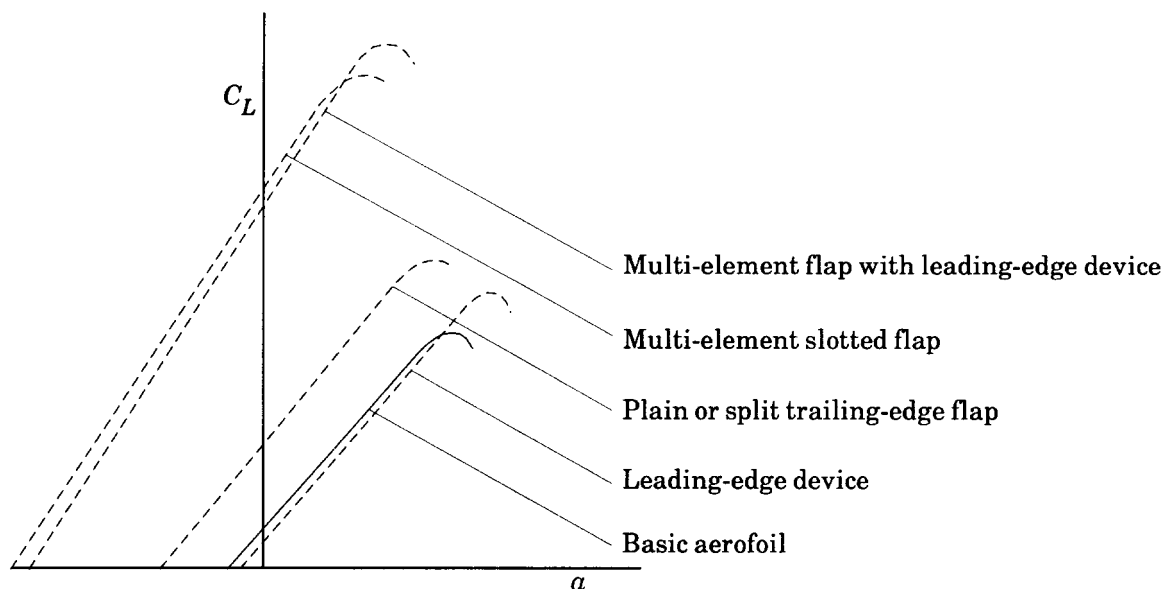
reducing the pressure gradient on the forward part of the main aerofoil section, thus allowing a higher angle of attack to be achieved before separation occurs in this region. If there is a chord extension there is a further rise in maximum lift coefficient.

Plain trailing-edge flaps (Sketch 3.3b) achieve higher maximum lift coefficients largely due to the camber effect which increases the lift coefficient at zero angle of attack. For large flap deflections the upper-surface suction has a maximum at the hinge line as well as at the leading edge. So the adverse pressure gradient over much of the aerofoil is reduced while over the flap it is greatly increased. As a result flow separation occurs over the flap at moderate deflections, but does not pass upstream of the hinge until much higher deflections are reached. Lift due to flap deflection continues to increase at a reduced rate, reaching a maximum just before separation moves ahead of the flap or the flow breaks down at the leading edge.
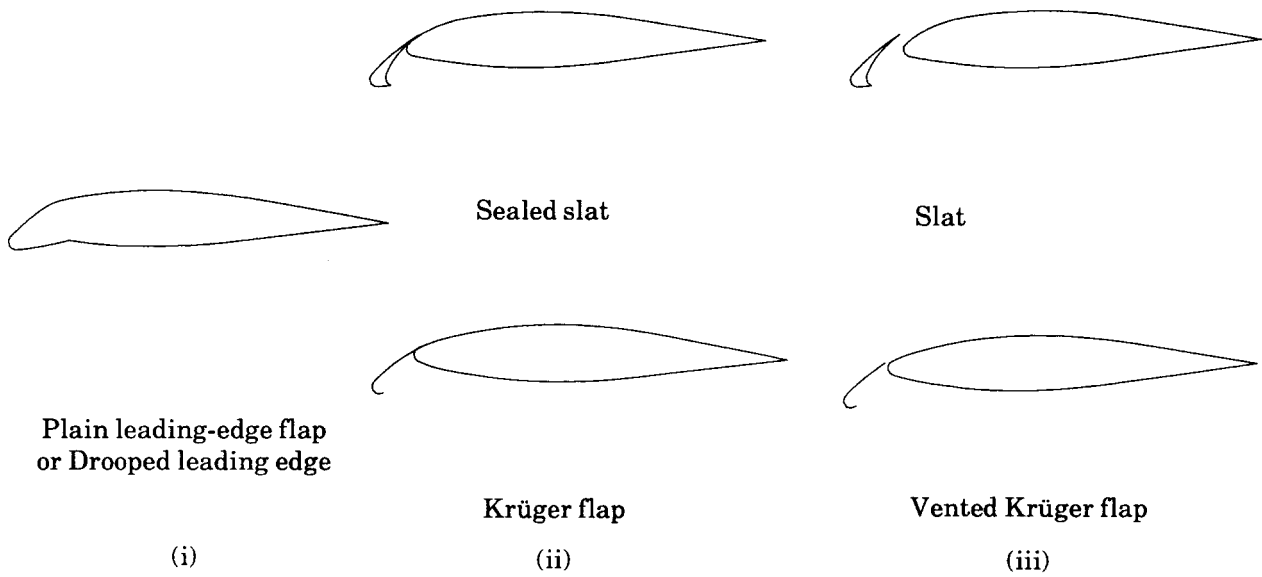
Deflection of a split flap (Sketch 3.3c) creates a region of low pressure behind the flap which depresses the aerofoil trailing-edge pressure. As a result a less adverse pressure gradient is created over the rear upper surface of the aerofoil, thus delaying the onset of trailing-edge separation and increasing the maximum lift coefficient. Therefore, separation may occur first at the leading edge of the aerofoil, in which case the lift would fall more sharply from the maximum.

Slotted trailing-edge flaps (Sketch 3.3d) develop considerably more maximum lift than plain flaps because the flow through the slot gives rise to a number of beneficial effects (see References 5 and 7). Fowler flaps (Sketch 3.3e) behave in a similar fashion to simple slotted flaps but develop more lift due to their greater chord extensions. Multi-element systems can employ a combination of the two types, although a wholly Fowler system is more efficient (Sketch 3.3e (iv), for example).
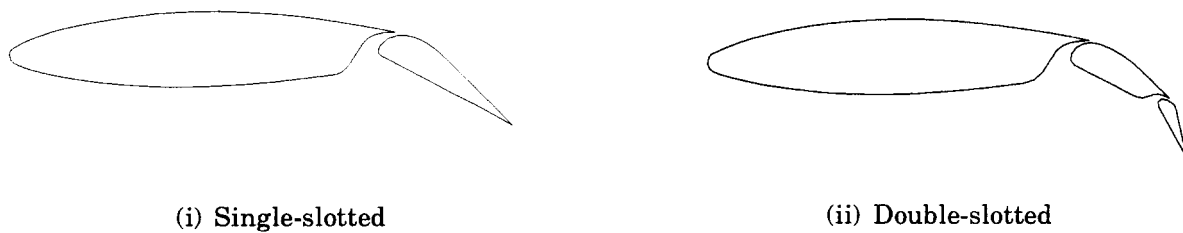
With a combination of leading-edge and trailing-edge devices (Sketch 3.3f), the highest practical values of C_{Lm} for mechanical systems are achievable as indicated in Sketch 3.2. The leading-edge device has essentially similar incremental effects whether or not the trailing-edge device is deflected.

Sketch 3.2   Typical lift curves

Sealed slat

Slat

Plain leading-edge flap
or Drooped leading edge

Krüger flap

Vented Krüger flap

(i)

(ii)

(iii)

a. Leading-edge devices

b. Plain flap

c. Split flap

(i) Single-slotted

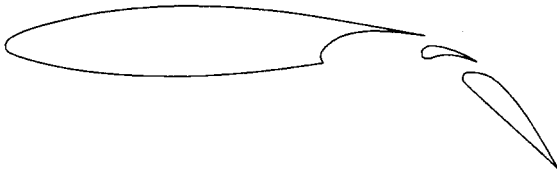(ii) Double-slotted

d. Simple slotted flaps

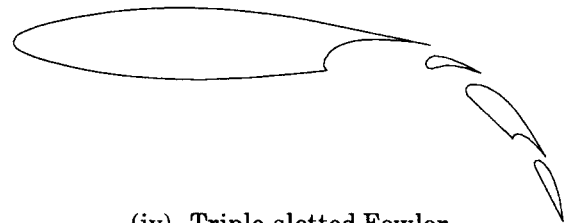**Sketch 3.3   Typical high-lift devices**
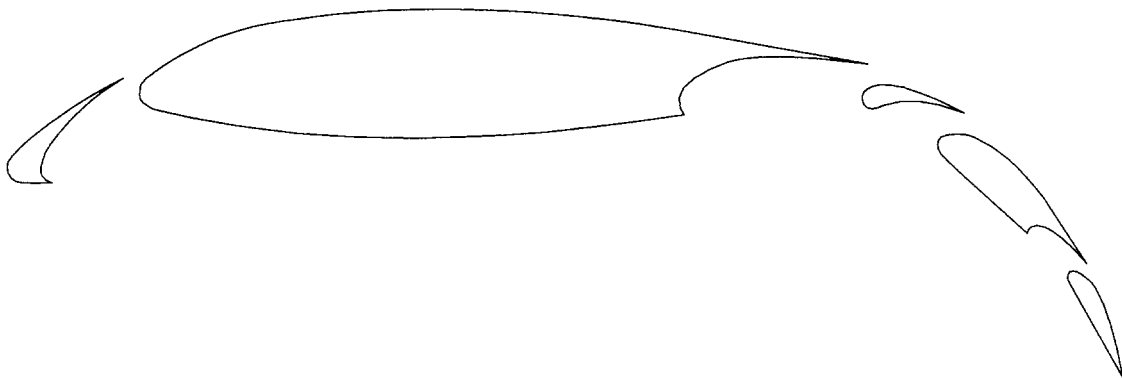
(i) Fowler

(ii) Tabbed Fowler

(iii) Vaned Fowler

(iv) Triple-slotted Fowler

e. Fowler flaps

f. Triple-slotted Fowler with slat

Sketch 3.3 Typical high-lift devices (Concluded)

3.2.1 Data Items

Further to Reference 6, a series of Data Items (References 8 to 12) has been developed for estimating the incremental effects, ΔC_{L0} and ΔC_{Lm}, of high-lift device deployment on C_{L0B} and C_{LmB}, for low speeds. The various methods were based on hinged thin-plate theory (Reference 4) with empirical correlation factors to account for the geometry of practical aerofoils and high-lift devices. To make some allowance for the effects of chord extension in the theory, the chord ratio of the high-lift device and the lift coefficient
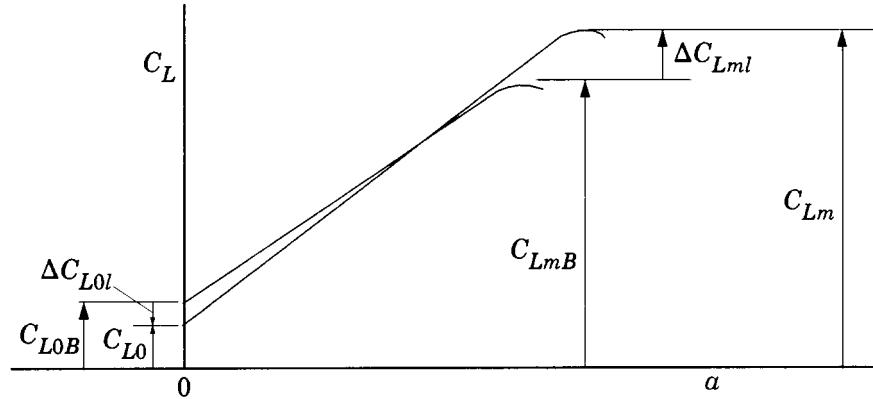
increments were based on the aerofoil extended chord, c'. For the case of slotted trailing-edge flaps further adjustments were required to adapt to the considerable departure from the thin hinged plate basis of the theoretical model due to slot effects and, possibly, large chord extensions. The resulting values of incremental lift coefficient are ultimately factored in the methods by c'/c to revert to the basic aerofoil chord as the reference length. The methods are suitable for low-speed flows with free-stream Mach numbers less than about 0.2. Whereas values of ΔC_{L0} are essentially independent of Reynolds number, values of ΔC_{Lm} are influenced by Reynolds number and, to account for that, the methods employ a simple Reynolds number dependent factor.

Item No. 94027 (Reference 8) treats a range of leading-edge high-lift devices, namely plain leading-edge flaps, drooped leading edges, slats (including sealed slats) and Krüger flaps (including vented Krügers). Trailing-edge flaps are treated in Item No. 94028 (Reference 9) for plain flaps, Item No. 94029 (Reference 10) for split flaps, Item No. 94030 (Reference 11) for single-slotted flaps and Item No. 94031 (Reference 12) for double-slotted and triple-slotted flaps. The flap types covered are those for which test data are available. However, the methods in References 11 and 12 for single-slotted and double-slotted trailing-edge flaps are capable of being adapted to other practical configurations incorporating a rear plain flap element. One such combination is the tabbed Fowler, which is a Fowler flap with a plain trailing-edge tab and Example 7.2 shows how this case can be addressed. This extended application should however be treated with some caution due to the lack of experimental evidence.
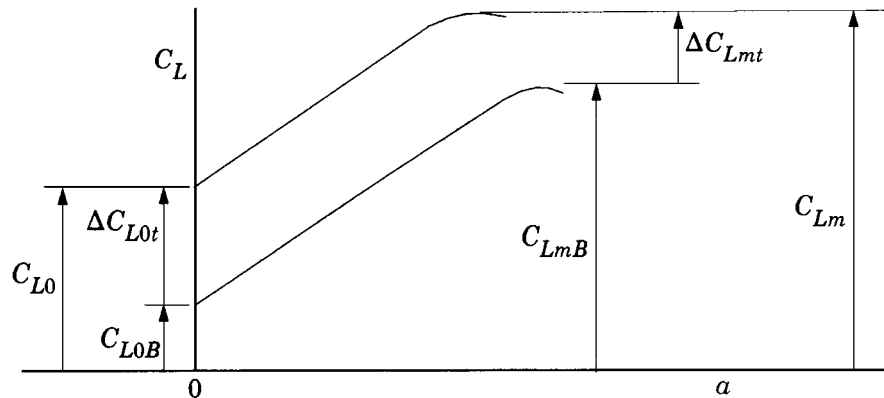
4. PROCEDURE FOR ESTIMATING C_{L0} AND C_{Lm}

Typical variations of lift coefficient with angle of attack at low speeds for an aerofoil with and without either a leading-edge device or a trailing-edge flap deployed are shown in Sketches 4.1a and 4.1b.

a. Leading-edge device

b. Trailing-edge flap

Sketch 4.1 Build up of C_{L0} and C_{Lm}

The principal aim of the sketches is to illustrate the build-up procedure for C_{L0} and C_{Lm}. From Sketch 4.1a it is seen that for an aerofoil with a leading-edge device deployed

$$C_{L0} = C_{L0B} + \Delta C_{L0l} \tag{4.1}$$

and
$$C_{Lm} = C_{LmB} + \Delta C_{Lml}. \tag{4.2}$$

It will be noted from Sketch 4.1a that ΔC_{L0l} has a negative value, as discussed in Section 3.2.

Similarly, from Sketch 4.1b, for an aerofoil with a trailing-edge flap deployed

$$C_{L0} = C_{L0B} + \Delta C_{L0t} \tag{4.3}$$

and
$$C_{Lm} = C_{LmB} + \Delta C_{Lmt}, \tag{4.4}$$

where ΔC_{L0t} and ΔC_{Lmt} are of a similar order of magnitude. All the lift coefficients in Equations (4.1) to (4.4) are based on the basic aerofoil chord, c.

For an aerofoil with a leading-edge device and a trailing-edge flap deployed the incremental effects can be combined to give

$$C_{L0} = C_{L0B} + \Delta C_{L0} \tag{4.5}$$

and

$$C_{Lm} = C_{LmB} + \Delta C_{Lm}, \tag{4.6}$$

where

$$\Delta C_{L0} = \Delta C_{L0l} + \Delta C_{L0t} \tag{4.7}$$

and

$$\Delta C_{Lm} = \Delta C_{Lml} + \Delta C_{Lmt}. \tag{4.8}$$

The assumption in Equations (4.7) and (4.8) is that there is no interference between the leading-edge and trailing-edge devices. The available evidence (see References 9 to 12) seems to support that inference for ΔC_{L0}. However, the evidence with regard to ΔC_{Lm} is not so conclusive, see Section 5.1. Guidance on the effect of interference on ΔC_{Lmt} is given, where possible, in the individual Data Items.

The values of C_{L0B} and C_{LmB} are estimated using the methods given in Item No.84026 (Reference 6).

The values of ΔC_{L0l} and ΔC_{Lml} for various leading-edge high-lift devices are obtainable from Item No. 94027 (Reference 8).

The values of ΔC_{L0t} and ΔC_{Lmt} for various trailing-edge flaps are obtainable from Item Nos 94028 to 94031 (References 9 to 12). Each of those Items includes at least two examples, one for an aerofoil with only the trailing-edge flap deployed, the other for the additional deployment of a leading-edge device.

Table 4.1 provides a guide to the locations of methods for the various contributions required in the evaluation of C_{L0} and C_{Lm} from Equations (4.1) to (4.8).

TABLE 4.1 Locations of information for determination of C_{L0} and C_{Lm}

High-lift devices		Parameters	Equation Nos	Item No.
Leading-edge	Trailing-edge			
none	none	C_{L0B}, C_{LmB}		84026
any	none	ΔC_{L0l}, ΔC_{Lml}	(4.1), (4.2)	94027
none	plain split single-slotted double-slotted triple-slotted	ΔC_{L0t}, ΔC_{Lmt}	(4.3), (4.4)	94028 94029 94030 94031 94031
any	plain split single-slotted double-slotted triple-slotted	ΔC_{L0}, ΔC_{Lm}	(4.5), (4.6) with (4.7), (4.8)	94027, 94028 94027, 94029 94027, 94030 94027, 94031 94027, 94031

5. APPLICABILITY AND ACCURACY

5.1 Applicability

The method of this Item is applicable to the estimation of the lift at zero angle of attack and the maximum lift for two-dimensional flow over aerofoils fitted with any of a range of leading-edge devices and trailing-edge flaps at low speeds. The types of leading-edge devices and trailing-edge flaps covered are detailed in Section 3.2.1 and are illustrated in Sketch 3.3. The methods for estimating each component in the build-up to C_{L0} and C_{Lm} are semi-empirical and a table giving the ranges of the various geometrical and flow parameters for the test data used in the development of the methods is given in each Data Item, see Table 4.1. These Items apply only to low-speed flows with free-stream Mach numbers less than about 0.2. Although there is no upper limit to the applicability in terms of Reynolds number, it is considered inadvisable to apply them to Reynolds numbers below 10^6 based on aerofoil chord for trailing-edge flaps and 0.6×10^6 for leading-edge devices.
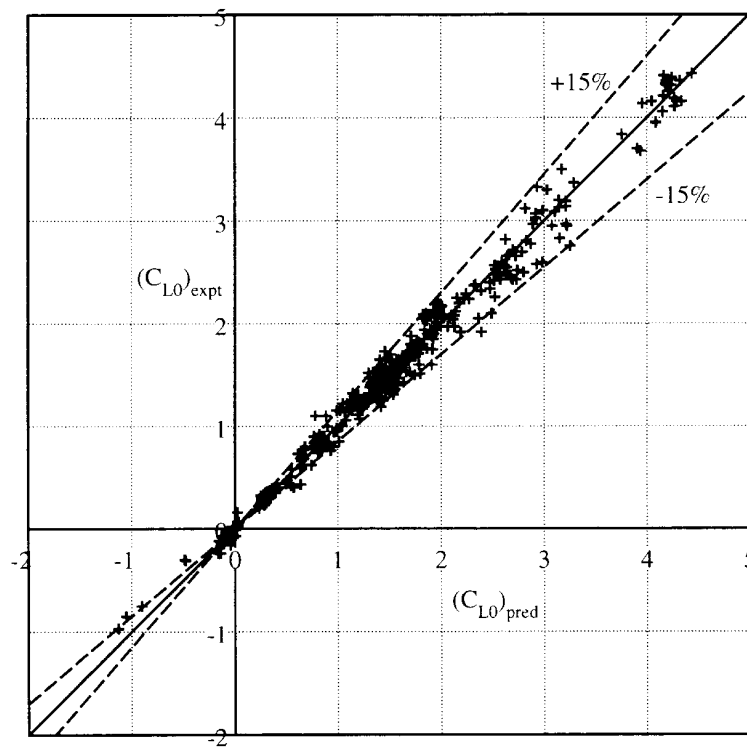
As noted in Section 4, there is some evidence to suggest that at maximum lift there can be some interference between the leading-edge device and a trailing-edge flap. The magnitude of the interference appears to depend on the trailing-edge flap type but is generally small – within the accuracy of the method for ΔC_{Lmt} for the case without leading-edge device deployment. Guidance on any interference effects is given where possible in the individual Data Items (References 9 to 12).

The influence of a slat or a slotted trailing-edge flap element on aerofoil lift, especially maximum lift, is crucially affected by the positioning of the slat or flap with respect to the aerofoil and by the shape of the slot involved. The methods for slats and slotted trailing-edge flaps (References 8, 11 and 12) take account, where possible, of the main effect of the slot gap. However, the configurations used in the analysis all had a reasonably well-designed convergent slot shape; poor slot shape can have a disastrous effect on ΔC_{Lm}.
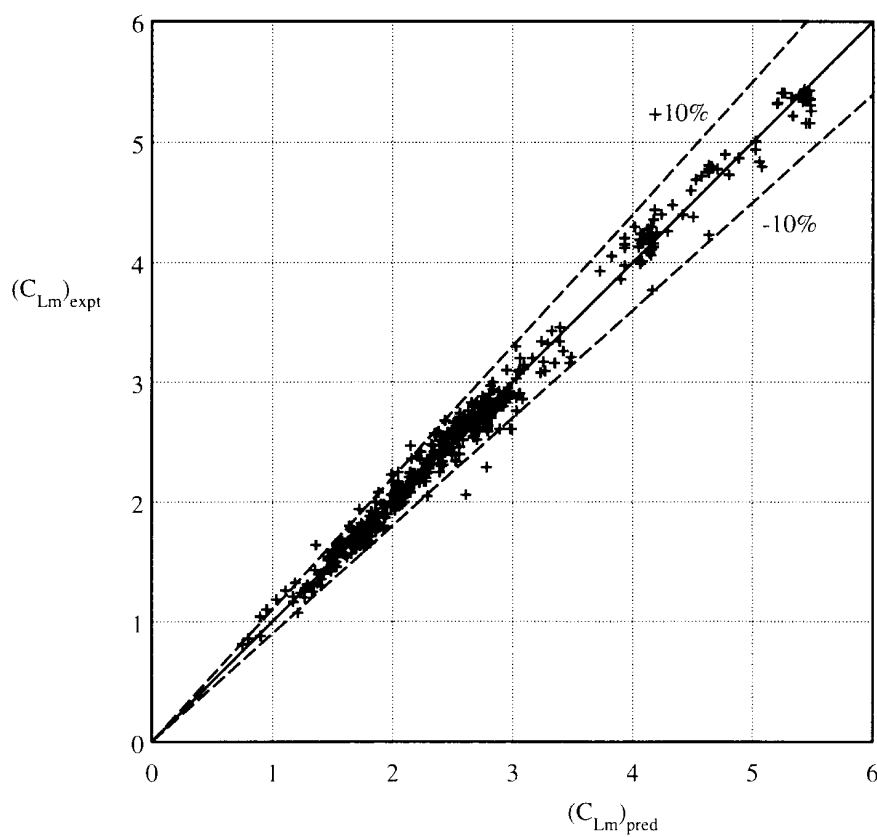
The methods of References 8, 11 and 12 should not be used as a basis for detailed optimisation studies. They are only intended to provide a realistic target for the maximum lift of a reasonably well-designed system.

5.2 Accuracy

Assessments of the accuracies of the prediction methods for the various components of C_{L0} and C_{Lm} are given in the associated Data Items (References 6 and 8 to 12). Sketches 5.1 and 5.2 show the comparisons between predicted and experimental values of C_{L0} and C_{Lm} respectively for the range of high-lift devices covered in the Data Items. It is seen that the predicted and test data for C_{L0} are, with few exceptions, correlated to within $\pm 15\%$; indeed nearly 80% were predicted to within $\pm 10\%$. In the case of C_{Lm} there is correlation to within $\pm 10\%$ for 97% of the 507 data points.

Sketch 5.1   Comparison of predicted and experimental values of C_{L0}

Sketch 5.2   Comparison of predicted and experimental values of C_{Lm}

6.   REFERENCES

The References are sources of information supplementary to that in this Item.

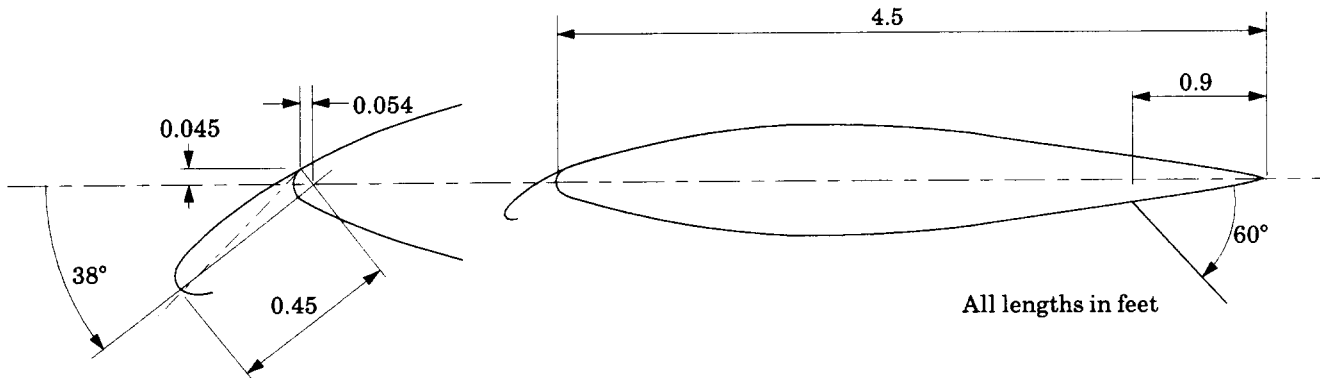| 1.	ESDU	The low-speed stalling characteristics of aerodynamically smooth aerofoils. ESDU International, Item No. 66034, 1966.
2.	HEBERT, J. *et al*.	Effects of high-lift devices on V/STOL aircraft performance. USAAVLABS tech. Rep. 70-33A, 1970.
3.	THAIN, J.A.	Reynolds number effects at low speeds on the maximum lift of two-dimensional aerofoil sections equipped with mechanical high lift devices. NAE (Div. Mech. Engng) *Quarterly Bulletin* No. 3, 1973.
4.	SCHEMENSKY, R.T.	Development of an empirically based computer program to predict the aerodynamic characteristics of aircraft. Volume 1: Empirical methods. Convair Aerospace Division, General Dynamics Corporation. AFFDL TR-73-144 (AD 780 100), 1973.
5.	SMITH, A.M.O.	High lift aerodynamics. *J. Aircraft*, Vol. 12, No. 6, June 1975.
6.	ESDU	Aerofoil maximum lift coefficient for Mach numbers up to 0.4. ESDU International, Item No. 84026, 1984.
7.	WOODWARD, D.S. LEAN, D.E.	Where is high-lift today? – A review of past UK research programmes. Paper No. 1 in AGARD CP 515, High-lift system aerodynamics, 1993.
8.	ESDU	Increments in aerofoil lift coefficient at zero angle of attack and in maximum lift coefficient due to deployment of various leading-edge high-lift devices at low speeds. ESDU International, Item No. 94027, 1994
9.	ESDU	Increments in aerofoil lift coefficient at zero angle of attack and in maximum lift coefficient due to deployment of a plain trailing-edge flap, with or without a leading-edge high-lift device, at low speeds. ESDU International, Item No. 94028, 1994.
10.	ESDU	Increments in aerofoil lift coefficient at zero angle of attack and in maximum lift coefficient due to deployment of a trailing-edge split flap, with or without a leading-edge high-lift device, at low speeds. ESDU International, Item No. 94029, 1994.
11.	ESDU	Increments in aerofoil lift coefficient at zero angle of attack and in maximum lift coefficient due to deployment of a single-slotted trailing-edge flap, with or without a leading-edge high-lift device, at low speeds. ESDU International, Item No. 94030, 1995.
12.	ESDU	Increments in aerofoil lift coefficient at zero angle of attack and in maximum lift coefficient due to deployment of a double-slotted or triple-slotted trailing-edge flap, with or without a leading-edge high-lift device, at low speeds. ESDU International, Item No. 94031, 1995.

7. EXAMPLES

7.1 Example 1

The lift coefficient at zero angle of attack and the maximum lift coefficient are to be estimated for a smooth NACA 65_2-015 aerofoil with a Krüger flap and a split flap deployed as shown in Sketch 7.1. In the notation of Item Nos 94027 and 94029 the relevant geometrical data are

Aerofoil	Krüger Flap	Split Flap
$c = 4.5$ ft	$c'_l = 0.45$ ft	$c_t = 0.9$ ft
$z_{cm}/c = 0$	$\delta^\circ_l = 38°(\delta_l = 0.663$ rad.$)$	$\delta^\circ_t = 60°(\delta_t = 1.047$ rad.$)$
$x_{lm}/c = 0.4$	$\rho_l/c = 0.015$	
$z_{lm}/c = -0.075$	$H_l = 0.045$ ft	
$z_{u1.25}/c = 0.017$	$x_\tau = 0.054$ ft	

and the flow conditions are

$$M = 0.1 \text{ and } R_c = 4.5 \times 10^6.$$

Sketch 7.1

The basic aerofoil has a symmetrical profile so that $C_{L0B} = 0$, and its maximum lift coefficient is estimated from Item No. 84026 to be

$$C_{LmB} = 1.37.$$

Table 4.1 shows that Equations (4.7) and (4.8) are appropriate, so that Equations (4.5) and (4.6) give

$$C_{L0} = C_{L0B} + \Delta C_{L0l} + \Delta C_{L0t}$$

and

$$C_{Lm} = C_{LmB} + \Delta C_{Lml} + \Delta C_{Lmt}$$

in which the increments due to the high-lift devices are estimated using Item No. 94027 for the Krüger flap in conjunction with Item No. 94029 for the split flap.

The values of ΔC_{L0l}, ΔC_{L0t} and ΔC_{Lml}, ΔC_{Lmt} for this example are calculated in Example 7.2 of Item No. 94029 so that

$$C_{L0} = 0 - 0.099 + 1.472 = 1.37$$

and $$C_{Lm} = 1.37 + 0.707 + 0.981 = 3.06.$$

7.2 Example 2

The lift coefficient at zero angle of attack and the maximum lift coefficient are to be estimated for a modified smooth NACA 65_2-215 aerofoil with a tabbed-Fowler flap and a slat deployed as shown in Sketch 7.2. The aerofoil, slat and Fowler flap are the same as those used in Example 8.2 of Item No. 94030. The required geometrical data are given in Sketch 7.2 using the notation of Item No. 94030, adapted to cover the addition of a plain flap.

The flow conditions are
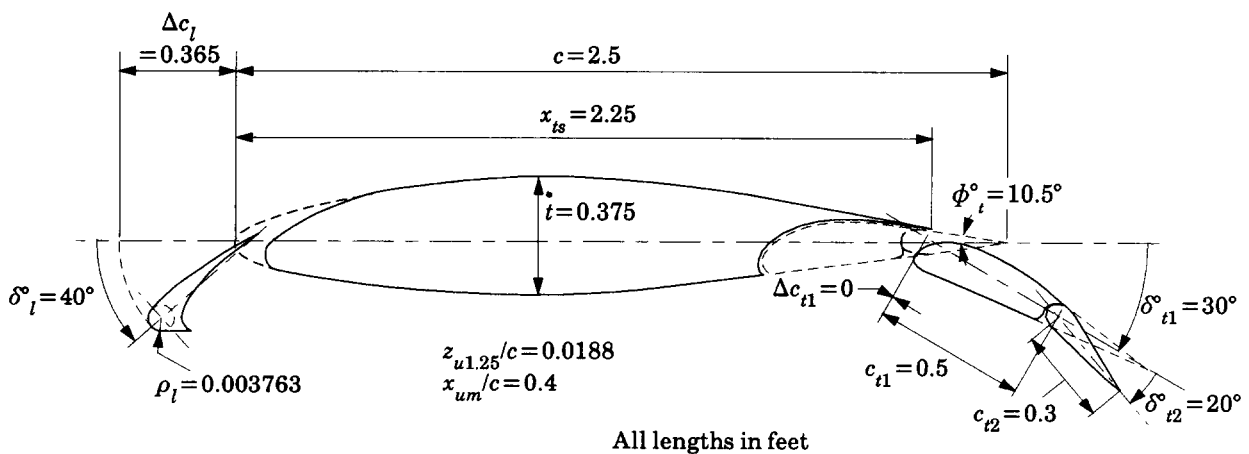
$$M = 0.2 \text{ and } R_c = 3.5 \times 10^6.$$

Also given for the modified NACA 65_2-215 are

$(a_1)_0 = 5.62 \text{ rad}^{-1}$ from Item No. Wings 01.01.05 for boundary-layer transition at the leading edge,

$C_{L0B} = 0.108$ from Item No. 84026,

and the datum value of C_{LmB}

$(C_{LmB})_d = 1.309$ from Item No. 84026 for a smooth aerofoil surface at $R_c = 3.5 \times 10^6$.

Sketch 7.2

As noted in the Introduction, the tabbed-Fowler flap will be treated by combining the methods of Item No. 94030 for a single-slotted flap and Item No. 94028 for a plain flap using the principles established for double-element flaps in Item No. 94031.

While working through the example, reference should be made to the individual Items for the notation and for details of the calculation.

With reference to Sketch 4.1 of Item No. 94031, the equivalent flap system to be used here is seen to consist of a single-slotted flap of chord c_{et1} coupled with a plain flap of chord c_{et2}. The equivalent single-slotted flap is treated using the method of Item No. 94030. The equivalent plain flap is treated using the method of Item No. 94028. With reference to Sketch 4.1 of Item No. 94031, the equivalent flap chords for the present system are evaluated as

$$
\begin{aligned}
c_{et1} &= c'_{t1} + c_{et2} \\
&= c_{t1} + \Delta c_{t1} + c_{et2} \\
&= c_{t1} + c_{t2} \\
&= 0.5 + 0.3 = 0.8 \text{ ft}
\end{aligned}
$$

and $\qquad c_{et2} = c_{t2} = 0.3$ ft,

since $c_{et2} = c_{t2}$ for a plain flap and $\Delta c_{t1} = 0$ for the present case.

Again by reference to Sketch 4.1 of Item No. 94031, the extended chord is given by

$$
\begin{aligned}
c' &= \Delta c_l + x_{ts} + c_{et1} \\
&= 0.365 + 2.25 + 0.8 \\
&= 3.415 \text{ ft,}
\end{aligned}
$$

giving $\qquad c'/c = 3.415/2.5 = 1.366,$

$$c_{et1}/c' = 0.8/3.415 = 0.234,$$

and $\qquad c_{et2}/c' = 0.3/3.415 = 0.0878.$

1. Trailing-edge Flap Contributions

(i) Contribution to ΔC_{L0}

(a) *Single-Slotted Flap* (Item No. 94030, Section 4.1)

Equation (4.3), for $\delta°_{t1} = 30°$, gives

$$J_{t1} = 1.17.$$

Figure 2, with $\delta°_{t1} = 30°$ and $c'_{t1}/c' (= c_{et1}/c') = 0.234$, gives

$$\Delta C'_{L1} = 1.193.$$

Therefore Equation (4.1) gives

$$\Delta C'_{L0t1} = J_{t1}\Delta C'_{L1}\,(a_1)_0/2\pi$$
$$= 1.17 \times 1.193 \times 5.62/2\pi$$
$$= 1.248.$$

(b)   *Plain Flap* (Item No. 94028)

Figure 1, with

$$\delta_t^\circ\ (= \delta^\circ{}_{t2}) + \phi_t^\circ = 20 + 10.5$$
$$= 30.5^\circ,$$

gives

$$J_p = 0.538\,.$$

Thus Equation (4.5), with $\delta_t = 20 \times \pi/180 = 0.349$ rad. and $c_t/c'(= c_{t2}/c') = 0.0878$, gives

$$\Delta C'_{L0t2} = 2J_p\delta_t\left\{\pi - \cos^{-1}(2c_{t2}/c' - 1) + [1 - (2c_{t2}/c' - 1)^2]^{\frac{1}{2}}\right\}$$

$$= 2 \times 0.538 \times 0.349 \times \left\{\pi - \cos^{-1}(2 \times 0.0878 - 1) + [1 - (2 \times 0.0878 - 1)^2]^{\frac{1}{2}}\right\}$$

$$= 0.439\,.$$

The total flap contribution is

$$\Delta C'_{L0t} = \Delta C'_{L0t1} + \Delta C'_{L0t2}$$
$$= 1.248 + 0.439$$
$$= 1.687\,,$$

which, in Equation (3.3) of Item No. 94030, gives

$$\Delta C_{L0t} = (c'/c)\Delta C'_{L0t}$$
$$= 1.366 \times 1.687$$
$$= 2.304\,.$$

(ii)   Contribution to ΔC_{Lm}

(a)   *Single-Slotted Flap* (Item No. 94030, Section 4.2)

Figure 3, with $z_{u1.25}/c = 0.0188$ and $x_{um}/c = 0.4$, gives

$$K_T = 2.5.$$

Figure 4, with $\delta^\circ_{t1} = 30°$, gives

$$K_{t1} = 0.35.$$

Equation (4.9) gives

$$\Delta C'_{Lmt1} = (1 - c/c')(1 - \sin\delta_{t1})(C_{LmB})_d + K_T K_{t1} J_{t1} \Delta C'_{L1},$$

which, with the values of J_{t1} and $\Delta C'_{L1}$ from (i), gives

$$\Delta C'_{Lmt1} = (1 - 1/1.366) \times (1 - \sin 30°) \times 1.309 + 2.5 \times 0.35 \times 1.17 \times 1.193$$
$$= 1.397.$$

(b) *Plain Flap* (Item No. 94028)

Figure 2, with
$$x'_s/c' = \tfrac{1}{2}c_{el}/c' = \tfrac{1}{2}c_l/c'$$
$$= \tfrac{1}{2} \times 0.046/3.415$$
$$= 0.0673$$

and $c_t/c' = c_{t2}/c' = 0.0878$, gives

$$T = 0.446.$$

Equation (4.9), with $\rho_l/t = 0.03763/0.375 = 0.1003$, gives

$$K_G = 1.225 + 4.525\rho_l/t$$
$$= 1.225 + 4.525 \times 0.1003$$
$$= 1.679,$$

and Equation (4.10) gives

$$K_t = 0.8.$$

Therefore, Equation (4.8), with $\Delta C'_{L0t2}$ from (i), gives

$$\Delta C'_{Lmt2} = K_G K_t T \Delta C'_{L0t2}$$
$$= 1.679 \times 0.8 \times 0.446 \times 0.439$$
$$= 0.263.$$

The total flap contribution is

$$\Delta C'_{Lmt} = \Delta C'_{Lmt1} + \Delta C'_{Lmt2}$$
$$= 1.397 + 0.263$$
$$= 1.660,$$

which, in Equation (3.4) of Item No. 94031, with $F_R = 1$ for $R_c = 3.5 \times 10^6$, gives

$$\Delta C_{Lmt} = F_R(c'/c)\Delta C'_{Lmt}$$
$$= 1 \times 1.366 \times 1.660$$
$$= 2.268 .$$

2. Slat Contributions

The slat geometry and the value of c' are identical to those in Example 8.2 of Item No. 94030. The slat contributions are therefore as calculated for that example, *i.e.*

$$\Delta C_{L0l} = 0.137 \quad \text{and} \quad \Delta C_{Lml} = 1.025 .$$

3. Total Values

Table 4.1 shows that Equations (4.7) and (4.8) are appropriate, so that Equations (4.5) and (4.6) give

$$C_{L0} = C_{L0B} + \Delta C_{L0l} + \Delta C_{L0t}$$
$$= 0.108 + (-0.137) + 2.304$$
$$= 2.28.$$

and $\quad C_{Lm} = C_{LmB} + \Delta C_{Lml} + \Delta C_{Lmt}$
$$= 1.309 + 1.025 + 2.268$$
$$= 4.60.$$

THE PREPARATION OF THIS DATA ITEM

The work on this particular Item, which supersedes, in part, Item No. 85033, was monitored and guided by the Aerodynamics Committee which first met in 1942 and now has the following membership:

Chairman
Mr H.C. Garner   – Independent

Members
Mr G.E. Bean[*]   – Boeing Commercial Airplane Company, Seattle, Wash., USA
Dr N.T. Birch   – Rolls-Royce plc, Derby
Dr P.C. Dexter   – British Aerospace plc, Sowerby Research Centre, Bristol
Mr J.R.J. Dovey   – Independent
Dr K.P. Garry   – Cranfield University
Mr D. Graham*   – Northrop Grumman Corp., Pico Rivera, Calif., USA
Mr M.J. Green   – Avro International Aerospace Ltd, Woodford
Dr H.P. Horton   – Queen Mary and Westfield College, University of London
Dr D.W. Hurst   – University of Southampton
Mr P.K. Jones   – Independent
Mr K. Karling*   – Saab-Scania AB, Linköping, Sweden
Mr M. Maurel   – Aérospatiale, Toulouse, France
Mr C.M. Newbold   – Aircraft Research Association, Bedford
Mr J.B. Newton   – British Aerospace Defence Ltd, Warton
Mr R. Sanderson   – Daimler-Benz Aerospace Airbus GmbH, Bremen, Germany
Mr A.E. Sewell*   – McDonnell Douglas Corp., Long Beach, Calif., USA
Mr M.R. Smith   – British Aerospace Airbus Ltd, Bristol
Mr J. Tweedie   – Short Brothers plc, Belfast.

[*]   Corresponding Member

The technical work in the assessment of the available information and the construction and subsequent development of the Data Item was carried out under contract to ESDU by Mr J.R.J. Dovey and by Mr P.D. Chappell, Head of the Aircraft Aerodynamics Group.